Title

Early Immunomodulatory Effects of Implanted Human Perivascular Stromal Cells During Bone Formation.

Journal

Tissue engineering. Part A, 24(5-6)

ISSN

1937-3341

Authors

Meyers, Carolyn A
Xu, Jiajia
Zhang, Lei
et al.

Publication Date

2018-03-01

DOI

10.1089/ten.tea.2017.0023

Peer reviewed

TISSUE ENGINEERING: Part A
Volume 24, Numbers 5 and 6, 2018

DOI: 10.1089/ten.tea.2017.0023

termis
Tissue Engineering
& Regenerative Medicine
International Society

ORIGINAL ARTICLE

Early Immunomodulatory Effects of Implanted Human Perivascular Stromal Cells During Bone Formation

Carolyn A. Meyers, BS,[1] Jiajia Xu, PhD,[1] Lei Zhang, MD, PhD,[1,2] Greg Asatrian, DDS,[3] Catherine Ding,[3] Noah Yan,[1] Kristen Broderick, MD,[4] Justin Sacks, MD,[4] Raghav Goyal, BS,[1] Xinli Zhang, MD, PhD,[3] Kang Ting, DMD, DMedSci,[3] Bruno Péault, PhD,[5,6] Chia Soo, MD, FACS,[6,7] and Aaron W. James, MD, PhD[1,6]

Human perivascular stem/stromal cells (PSC) are a multipotent mesodermal progenitor cell population defined by their perivascular residence. PSC are most commonly derived from subcutaneous adipose tissue, and recent studies have demonstrated the high potential for clinical translation of this fluorescence-activated cell sorting-derived cell population for bone tissue engineering. Specifically, purified PSC induce greater bone formation than unpurified stroma taken from the same patient sample. In this study, we examined the differences in early innate immune response to human PSC or unpurified stroma (stromal vascular fraction [SVF]) during the *in vivo* process of bone formation. Briefly, SVF or PSC from the same patient sample were implanted intramuscularly in the hindlimb of severe combined immunodeficient (SCID) mice using an osteoinductive demineralized bone matrix carrier. Histological examination of early inflammatory infiltrates was examined by hematoxylin and eosin and immunohistochemical staining (Ly-6G, F4/80). Results showed significantly greater neutrophilic and macrophage infiltrates within and around SVF in comparison to PSC-laden implants. Differences in early postoperative inflammation among SVF-laden implants were associated with reduced osteogenic differentiation and bone formation. Similar findings were recapitulated with PSC implantation in immunocompetent mice. Exaggerated postoperative inflammation was associated with increased *IL-1α, IL-1β, IFN-γ*, and *TNF-α* gene expression among SVF samples, and conversely increased *IL-6* and *IL-10* expression among PSC samples. These data document a robust immunomodulatory effect of implanted PSC, and an inverse correlation between host inflammatory cell infiltration and stromal progenitor cell-mediated ossification.

Keywords: perivascular stem cell, PSC, mesenchymal stromal cell, mesenchymal stem cell, MSC, immunomodulation

Introduction

Rouget first described the mural cells of capillary walls. Nearly fifty years thereafter, Zimmermann renamed these cells as pericytes and described their contractile function.[1] Scattered observations described the possible multipotentiality of pericytes, including an ability to undergo differentiation to other mesenchymal cell lineages.[2–4] For example, Covas *et al.* identified mesenchymal stem/stromal cell (MSC)-like cells within human veins, but did not show their location.[5] It was not until Crisan *et al.* utilized a combination of immunohistochemical and flow cytometry analysis that the MSC identity of pericytes was fully appreciated.[6] Since this time, multiple independent investigators have confirmed the MSC attributes of pericytic/perivascular cells (see Murray *et al.*[7] for a review). In addition, several groups have identified pericytes as progenitor cells involved in endogenous tissue repair.[8–10] In summary,

[1]Department of Pathology, Johns Hopkins University, Baltimore, Maryland.
[2]Department of Oral and Maxillofacial Surgery, School of Stomatology, China Medical University, Shenyang, PR China.
[3]Section of Orthodontics, Division of Growth and Development, School of Dentistry, University of California, Los Angeles, Los Angeles, California.
[4]Department of Plastic Surgery, Johns Hopkins University, Baltimore, Maryland.
[5]Center for Cardiovascular Science and MRC Center for Regenerative Medicine, University of Edinburgh, Edinburgh, United Kingdom.
[6]UCLA Orthopedic Hospital Department of Orthopedic Surgery and the Orthopedic Hospital Research Center, Los Angeles, California.
[7]Division of Plastic and Reconstructive Surgery, Department of Surgery, David Geffen School of Medicine, University of California, Los Angeles, Los Angeles, California.

multiple investigators have defined the perivascular residence of MSC-like cells.

Since the original description of adipose tissue as a source of multilineage stromal cells,[11] the preclinical study of adipose-derived cells for tissue engineering has increased dramatically (reviewed in Zuk[12]). The theoretical advantages of adipose-derived cells over other cell types for bone tissue engineering strategies are multiple, including ease of access, low donor-site morbidity, as well as a high cell proliferative rate and robust osteogenic differentiation potential. Nevertheless, the stromal vascular fraction (SVF) of adipose tissue is a heterogeneous cell population composed of perivascular cells, inflammatory cells, other stromal cells, and endothelium. To address this issue of SVF heterogeneity, previous investigators have used fluorescence-activated cell sorting (FACS) to purify adipose-derived cell populations, with some success in tissue engineering approaches. For example, cell sorting of adipose tissue has allowed for enrichment of ''osteoprogenitor,''[13] or ''chondroprogenitor''[14] cell types, but not the isolation of multipotent MSC. In summary, although previous studies have sought to enrich mesenchymal progenitor cells within adipose-derived SVF, this was not a prospective isolation based on cell identity.

To address the issue of heterogeneity within the SVF, we previously purified a population of MSC termed perivascular stem/stromal cells (PSC) from the SVF of human white adipose tissue.[15] PSC are purified by FACS and are a relatively homogenous MSC starting population for regenerative applications.[16,17] PSC are abundant in human subcutaneous adipose tissue and are present in high numbers (representing $\sim$40% of viable SVF).[17] Importantly, PSC are identified and derived without culture expansion.[16,18] PSC originate in the vessel wall[6,7] and are composed of two related cell populations, including pericytes ($CD34^-CD146^+CD45^-$) and adventitial cells ($CD34^+CD146^-CD45^-$).[6,19] Additional characteristic cell surface markers of PSC include CD10, CD13, CD44, CD73, CD90, and CD105.[15] In comparison with cells of the SVF from the same patient, PSC have shown significantly greater potential for bone formation by their ability to form bone in an intramuscular implantation model.[17,20] Additionally, PSC have been shown to promote *in vivo* bone regeneration across other animal models, including a rat spinal fusion model,[16,20] and a calvarial defect model in mice.[21]

To date, the positive bone-forming attributes of PSC have not been examined in the context of their immunomodulatory attributes. Endogenous pericytes possess natural immunoregulatory effects across diverse organ systems, observed in the brain,[22–24] heart,[25] placenta,[26] and tumor-associated vasculature.[27] Indeed, accumulating evidence suggests that pericytes are immunoregulatory effector cells with diverse roles in antigen presentation,[28,29] regulation of $CD4^+$ T cell activation and proliferation,[26,27,30] and T cell anergy.[27] In a recent tissue engineering model, pericyte transplantation in a mouse cardiac injury reduced leukocyte and macrophage accumulation.[31] These immunomodulatory effects resulted in improved cardiomyocyte survival and improved contractility.[31] Despite the immunomodulatory effects of pericytes and perivascular cells in other organs and model systems, these effects during the process of PSC-mediated bone formation have remained undefined. In this study, we utilize our previously established mouse intramuscular implantation model[17] to examine how implanted PSC exert effects on the innate immune system during the early postoperative period.

Materials and Methods

PSC isolation

PSCs were purified by FACS of the human SVF as previously described.[17] SVF was incubated with a mixture of the following directly conjugated antibodies: anti-$CD34^-$ allophycocyanin (1:60; BD Biosciences,), anti-$CD45^-$ allophycocyanin-cyanine7 (1:60; Santa Cruz Biotechnology, Inc., Santa Cruz, CA), and anti-$CD146^-$ fluorescein isothiocyanate (1:30; AbD Serotec, Raleigh, NC). All incubations were performed at 4°C for 15 min in the dark. Before sorting, 4′,6-diamidino-2-phenylindole (DAPI, 1:1000; Invitrogen, Carlsbad, CA) was added for dead cell exclusion; the solution was then passed through a 70-μm cell filter and then run on a FACSAria cell sorter (BD Biosciences, San Diego, CA). Sorted cells were used for *in vivo* application immediately or plated for *in vitro* studies. In this manner, distinct microvessel pericytes ($CD146^+CD34^-CD45^-$) and adventitial cells ($CD34^+CD146^-CD45^-$) were isolated and combined to constitute the PSC population. See Supplementary Table S1 for a list of antibodies used for cell isolation (Supplementary Data are available online at www.liebertpub.com/tea).

In vitro *osteogenic differentiation assay*

Alkaline phosphatase staining was performed using the Leukocyte Alkaline Phosphatase Kit (Sigma-Aldrich). Briefly, cells were seeded in six-well plates at 100,000 cells/well. After 24 h, medium was changed to either standard growth medium (Dulbecco's modified Eagle's medium [DMEM] + 10% fetal bovine serum [FBS]) or osteogenic differentiation medium composed of 10 mM β-glycerophosphate and 50 μM ascorbic acid in DMEM +10% FBS. After 5 days of osteogenic differentiation, cells were washed with phosphate-buffered saline (PBS) and fixed with formalin for 10 min at room temperature. Following fixation, cells were stained using the Leukocyte Alkaline Phosphatase Kit (Sigma-Aldrich) according to the manufacturer's protocol. Cells were incubated in alkaline phosphatase for 30 min at room temperature, then washed with water. Cells were allowed to dry and images were captured at 4× magnification.

RNA isolation and quantitative real-time polymerase chain reaction

Ribonucleic acid was extracted from freshly isolated, patient-matched SVF and PSC samples using the RNEasy Kit (Qiagen, Santa Clarita, CA). One microgram of total RNA from each sample was subjected to first-strand complementary DNA (cDNA) synthesis using the iScript cDNA Synthesis Kit (Bio-Rad Laboratories, Hercules, CA). The reverse transcription was performed at 25°C for 5 min, 46°C for 20 min, followed by 95°C for 1 min. For quantitative real-time polymerase chain reaction (qRT-PCR), the reaction was performed using 2× SYBR Green RT-PCR Master Mix and a Bio-Rad CFX96™ Touch Real-Time PCR Detection System (Bio-Rad Laboratories). The primers used are listed in Supplementary Table S2. qRT-PCR was performed using 96-well optical plates at 95°C for 10 min, followed by 50 cycles at

95°C for 15 s, and at 60°C for 60 s. The relative quantification of gene expression was performed using a comparative CT method according to the manufacturer's protocol and was normalized to the expression levels of *ACTB* in each sample.

Implant preparation

Implant preparation was performed as previously described.[17] A DBX Putty was used (100 μL; Musculoskeletal Transplant Foundation, Edison, NJ). DBX Putty combines morselized cortical–cancellous demineralized bone chips with sodium hyaluronate, and it was chosen for its proven osteoinductive characteristics.[32,33] Defined numbers of viable cells in PBS suspension (2.5×10^5 cells in 20 μL) from the human SVF or PSC were mechanically mixed with the DBX scaffold. The cell + scaffold suspension was kept on ice until implantation (<45 min). In select studies, a collagen sponge carrier (Medtronic, Minneapolis, MN) was used ($2 \times 1 \times 0.5$ cm sponge loaded with 2.5×10^5 PSC). Scaffold alone was used as a further control.

Surgical procedures

Intramuscular implantation was performed as previously described in 8-week-old male severe combined immunodeficiency (SCID) mice.[17] Briefly, animals were anesthetized by isoflurane inhalation and premedicated with buprenorphine. Bilateral incisions in the hindlimbs were made, and pockets were cut in the biceps femoris muscles by blunt dissection, parallel to the muscle fiber long axis. Dissection methods and the surgical manipulation of tissues were kept as constant as possible across animals. The number of animals per experiment can be found in the figure legends. After implantation of the cell + scaffold composite, the fasciae overlying the muscle were sutured with a simple continuous pattern, and the skin was closed in a separate layer using 5-0 Vicryl (Ethicon, San Angelo, TX). Animals were postoperatively treated with buprenorphine. Animals were monitored for possible wound infection throughout the study period, with no significant findings. Surgeons were blinded to the experimental treatment groups during the procedure. Animals were housed and experiments were performed in accordance with guidelines of the Chancellor's Animal Research Committee of the Office for Protection of Research Subjects at the University of California, Los Angeles. In select studies, C57BL/6 immunocompetent mice were used.

Postoperative imaging

Postoperative imaging was by high-resolution roentgenography (XR) and microcomputed tomography (microCT), based on our previously described methods.[17] Briefly, live high-resolution radiographs were taken at 2 weeks for select experiments using a cabinet radiography system (Faxitron Bioptics, Lincolnshire, IL). Postmortem high-resolution microCT was performed 4 weeks postoperatively (Skyscan 1172F; Skyscan, Kontich, Belgium) at an image resolution of 19.73 μm and analyzed using DataViewer, Recon, CTAn, and CTVol programs provided by the manufacturer.[17]

Histology and immunohistochemistry

Samples were formalin fixed, decalcified in 19% EDTA, and embedded in paraffin. Hematoxylin and Eosin (H&E) staining was performed. For select experiments, inflammatory cell composition was quantified by blinded histomorphometric analyses using random 20× images of the implantation site or periimplantation site soft tissues. Immunohistochemistry was performed with primary antibodies against Ly-6G (1:500; BioLegend) and F4/80 (1:200; Bio-Rad), using the ABC (Vector Laboratories, Burlingame, CA) method. Sections of mouse spleen and mouse bone marrow were used as staining controls. Select quantification of immunohistochemistry was performed either by manually counting the number of immunoreactive cells per high-power field, or using the magic wand tool in Photoshop to derive a relative staining intensity per image, using a tolerance setting of 30. For either method, 10 random high-power images per sample were analyzed, taken from either the implant substance or the peri-implant soft tissue. All images were taken and data analyzed in a blinded fashion.

Statistical analyses

All results were expressed as mean ± standard deviation. Statistical analyses were performed using the SPSS16.0 software. All data were normally distributed. Student's *t*-test was used for two-group comparisons and Benjamini–Hochberg corrections were used for multiple testing (false discovery rate = 0.05). One-way ANOVA test was used for comparisons of three or more groups, followed by Tukey's *post hoc* test. Differences were considered significant when $p < 0.05$.

Results

PSC isolation and bone formation

First, PSC were purified from human lipoaspirate, based on differential expression of CD146 and CD34 (Fig. 1). Briefly, using previously established protocols, the SVF of lipoaspirate was processed so as to remove $DAPI^+$ nonviable cells (Fig. 1A), as well as $CD45^+$ hematopoietic cells (Fig. 1B). Next, pericytes were defined as a $CD146^+CD34^-CD45^-$ cell population, whereas adventitial progenitor cells are $CD34^+CD146^-CD45^-$ (Fig. 1C). When combined, this bipartite population is termed PSC and is characterized by expression of characteristic MSC markers and lack expression of hematopoietic or endothelial cell markers.[6,18,19] Prior studies have confirmed that PSC have multilineage differentiation potential, including an ability to differentiate down osteogenic, adipogenic, myogenic, and chondrogenic lineages.[6,19] Here, the osteogenic differentiation potential of PSC was further confirmed *in vitro* and *in vivo* (Fig. 1D, E). After 5 days under standard osteogenic differentiation conditions, PSC in monolayer culture demonstrated robust enzymatic activity for alkaline phosphatase (Fig. 1D). PSC-induced ectopic bone formation was next assessed, using an intramuscular implantation model in the hindlimbs of SCID mice (Fig. 1E). Over the course of 2 weeks, ectopic ossification of a collagen sponge implant was noted in the PSC-loaded implant site.

Previously, we reported that in a mouse hindlimb intramuscular implantation assay, implanted PSC led to significant greater ectopic bone formation in comparison to unpurified SVF derived from the same patient sample.[17] We sought to confirm these findings, using a demineralized bone matrix (dbm) carrier and equal amounts of SVF or PSC from the same patient sample. At 4 weeks postimplantation, ectopic bone formation was assessed by microCT imaging and three-dimensional

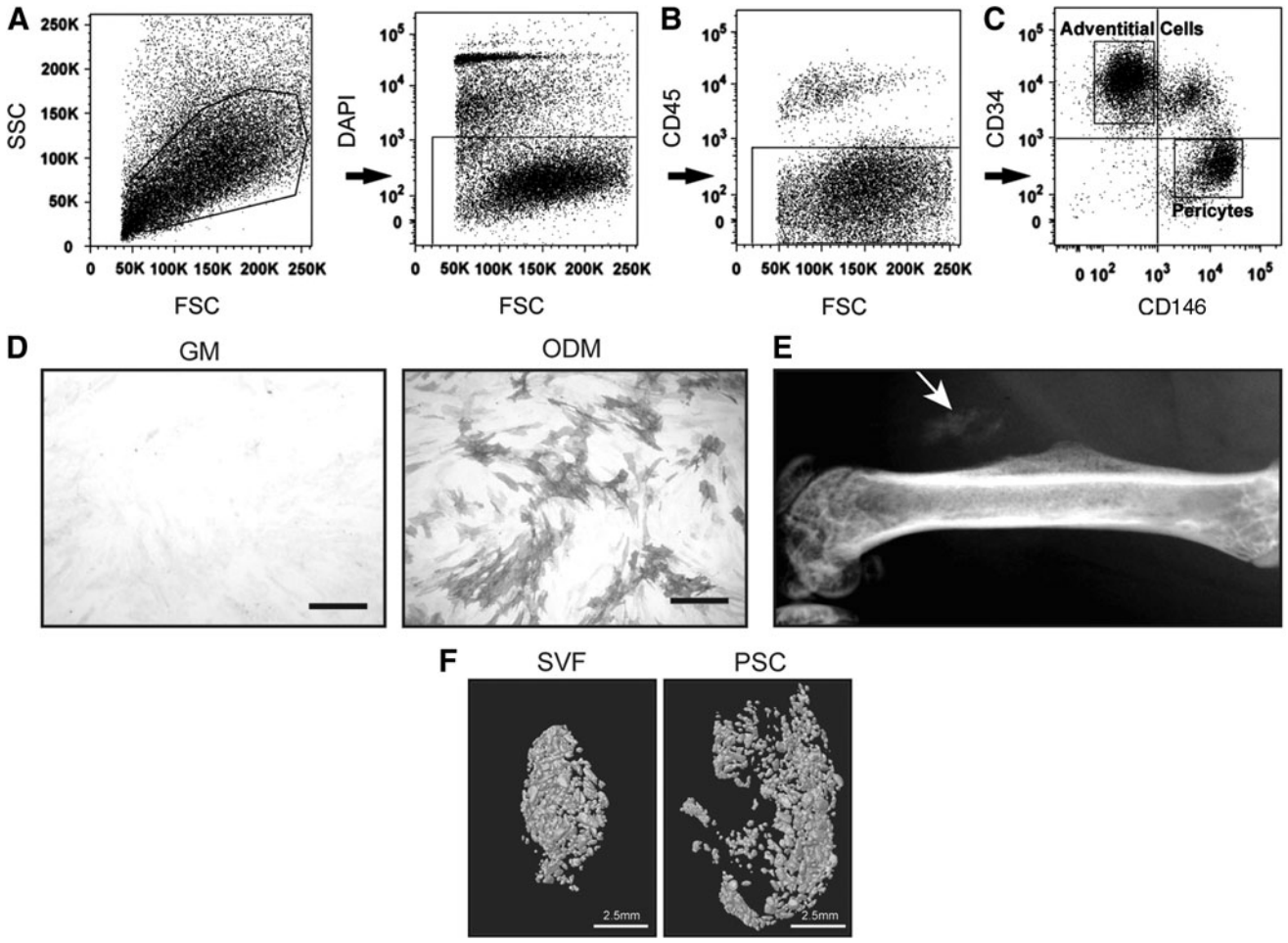

FIG. 1. Human PSC isolation and bone formation. **(A–C)** Fluorescence-activated cell sorting (FACS) isolation for PSC. **(A)** First, $DAPI^+$ nonviable cells and **(B)** $CD45^+$ inflammatory cells were excluded from the SVF of human lipoaspirate. **(C)** Next, purified PSC were obtained based on differential expression of CD146 and CD34 within the $CD45^-$ cell population. Based on prior studies, pericytes are defined as a $CD146^+CD34^-CD45^-$ population, whereas $CD34^+CD146^-CD45^-$ are an adventitial progenitor cell population. Together, these two cell populations comprise the bipartite population, PSC. **(D)** PSC were cultured using standard GM (*left*) and ODM (*right*) in monolayer. Alkaline phosphatase staining at 5 days. Scale bar (*black*) = 25 μM. **(E)** After isolation, PSC were implanted intramuscularly on a collagen sponge carrier in SCID mice. After 2 weeks, ectopic bone formation was observed. **(F)** Differential bone formation of SVF and PSC. Finding of prior studies was confirmed,[17] demonstrating that PSC induced significantly greater ectopic bone formation than SVF derived from the same patient sample. Scale bar (*white*) = 2.5 mm. Microcomputed tomography reconstructions of ectopic bone formation are visualized 4 weeks after cell implantation. $n = 6$ implants per cell treatment. **(A–C)** Reproduced with permission from Askarinam *et al.*[22] DAPI, 4′,6-diamidino-2-phenylindole; FSC, forward scatter; GM, growth medium; ODM, osteogenic differentiation medium; PSC, perivascular stem/stromal cells; SCID, severe combined immunodeficiency; SSC, side scatter; SVF, stromal vascular fraction.

reconstructions (Fig. 1F). In agreement with our prior observations,[17] patient-matched PSC led to significantly greater ectopic bone formation. In our prior observations, the percentage increase in bone formation when comparing PSC to SVF ranged from a 15–80% increase depending on the variable examined.[17] Across all variables, PSC-treated implants led to greater bone formation than acellular control (scaffold alone).[20]

Immunomodulatory effects of PSC in ectopic bone formation model

To better understand the different bone formation outcomes induced by purified PSC versus SVF, we repeated our previously devised model–now examining an early postoperative time point. At 1 week postoperatively, implants were examined for histological appearance. At low magnification, all implants remained embedded within the skeletal muscle (m), and in proximity to the underlying femur (f) (Fig. 2A, B). Even at low magnification, SVF-laden implants showed greater amounts of granulation tissue (gt) surrounding the implant site. As expected in a surgical model, significant spatial variation in histological appearance was observed. To best evaluate, we examined the implant site and peri-implant soft tissues individually (Fig. 2C–H). Within the implant site, both SVF- and PSC-laden implants had an overall similar histological appearance, characterized by dbm particles embedded in a fibrovascular stroma with extravasated red blood cells (Fig. 2C, D). However, the fibrovascular stroma was more hypercellular in SVF-treated implants, and more detailed analysis showed an overall increase in polymorphonuclear leukocytes (circled, Fig. 2C, D).

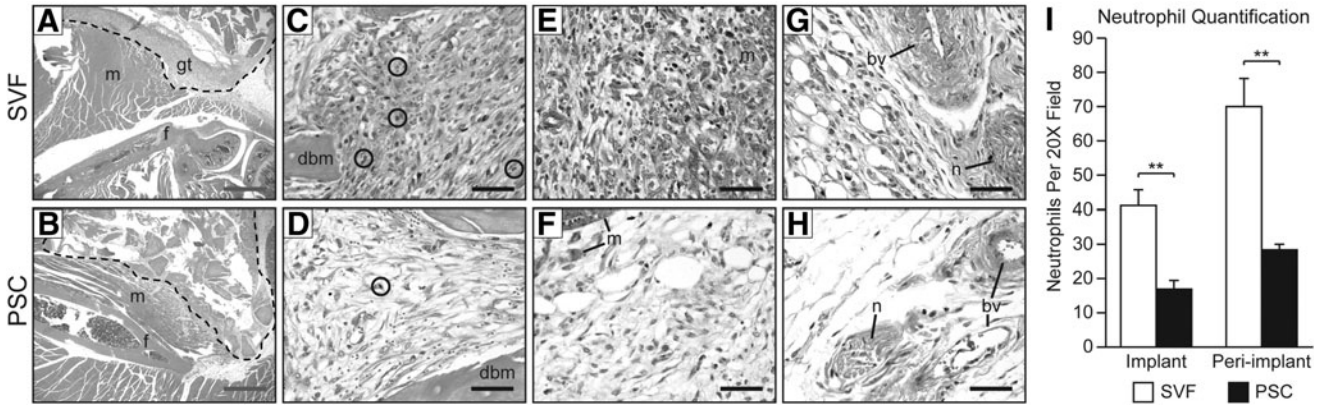

FIG. 2. Early histological appearance after SVF or PSC intramuscular implantation. **(A, B)** Low magnification images of hematoxylin and eosin staining to illustrate representative histological appearance, 1 week postoperative. The implant area (encircled by *dashed lines*) is bounded by skeletal muscle (m) in all samples. A notable increase in peri-implant granulation tissue (gt) is seen among SVF-laden implants. 2× images. Scale bar (*blue*) = 500 μM. **(C, D)** High-magnification images of the implant site, 1 week postoperatively. *Circles* highlight polymorphonuclear leukocytes. 40× images. Scale bar (*black*) = 25 μM. **(E, F)** High-magnification images of the immediate peri-implant site, 1 week postoperatively. 40× images. Scale bar (*black*) = 25 μM. **(G, H)** High-magnification images of the peri-implant adipose tissue more distant from the implant site, 1 week postoperatively. 40× images. Scale bar (*black*) = 25 μM. **(I)** Quantification of polymorphonuclear leukocyte number, as assessed per random 20× field within the implant site and immediate peri-implant areas. $^{**}p < 0.01$. $n = 4$ implants per cell treatment; $n = 10$ images analyzed per sample. bv, blood vessel; dbm, demineralized bone matrix; f, femur; gt, granulation tissue; m, muscle; n, nerve; svf, stromal vascular fraction; psc, perivascular stem/stromal cell.

Analysis of the immediate peri-implantation site highlighted similar differences (Fig. 2E, F). Here, adjacent to SVF-laden implants were larger foci of granulation tissue characterized by a dense acute and chronic inflammatory cell infiltrate, enlarged, reactive-appearing fibroblast-like cells, and a proliferation of slender capillary-type vessels (Fig. 2E). In contrast, in PSC-laden implants, a similar cell composition was observed, including fibroblasts, capillary endothelium, and inflammatory cells, but the density of inflammatory cells was much reduced (Fig. 2F). Differences in the histological appearance of SVF and PSC-laden implants were even observed in the peri-implant adipose tissue at some distance removed from the intramuscular site (Fig. 2G, H). Here and among SVF-treated samples, scattered mononuclear and polymorphonuclear inflammatory cells were observed in the peri-implant adipose tissue, most notably adjacent to neurovascular structures (Fig. 2G). The degree of inflammation within adipose tissue and associated neurovascular structures was less prominent among PSC-treated samples (Fig. 2H).

The most striking difference in cell composition between implants was the degree of polymorphonuclear leukocyte (neutrophilic) infiltration. Quantification of random high-power fields was performed in a blinded fashion to assess the degree of neutrophilic infiltrate within the implant site and immediate peri-implantation areas (Fig. 2I). Results showed a significant attenuation of neutrophils within both areas in PSC-treated implants.

PSC implantation reduces Ly-6G$^+$ cell infiltration

Next, Ly-6G (lymphocyte antigen 6 complex, locus G; also termed myeloid differentiation antigen Gr-1) expression was examined (Fig. 3). Ly-6G is expressed in peripheral neutrophils as well as the majority of myeloid cells within the bone marrow. Ly-6G expression was examined 1 week after SVF or PSC intramuscular implantation. Within the implant site and in agreement with our H&E staining observations, a higher density of Ly-6G$^+$ cells was observed in the fibrovascular stroma of SVF-treated samples (Fig. 3A, B). The peri-implant soft tissue showed a similar difference among SVF and PSC-treated samples, with a significant increase in density of Ly-6G$^+$ cells within SVF-laden samples (Fig. 3C, D). Expected Ly-6G staining patterns within the murine bone marrow and spleen were confirmed (Fig. 3E, F). Finally, quantification of Ly-6G$^+$ cell numbers was performed, either in the implant site or peri-implant soft tissues (Fig. 3G). Results showed a significant reduction in Ly-6G$^+$ cell number within PSC-treated samples, both within the implant and peri-implant tissues.

PSC implantation reduces F4/80$^+$ cell infiltration

Next, F4/80 was examined as a marker of murine macrophage populations (Fig. 4). F4/80 expression was again examined 1 week after SVF or PSC intramuscular implantation. Within the implant site, rare F4/80$^+$ cells were identified within the fibrovascular stroma, usually adjacent to demineralized bone chips (dbm) (Fig. 4A, B). In contrast, the immediate peri-implant site showed a band of F4/80 immunoreactive cells encircling the implant site within both SVF and PSC treatment groups (Fig. 4C, D, dashed lines indicate margins of band-like staining). Among SVF-treated samples, the band of peri-implant F4/80$^+$ cells was generally wider and with greater distribution of stain. As a positive control, the expected staining patterns for F4/80 were observed within the murine periosteum and spleen (Fig. 4E, F). Finally, semiquantification of F4/80 staining intensity was performed, again either in the implant site or peri-implant soft tissues (Fig. 4G). Results showed a significant relative reduction in F4/80 staining within PSC-treated samples within both the implant and peri-implantation sites.

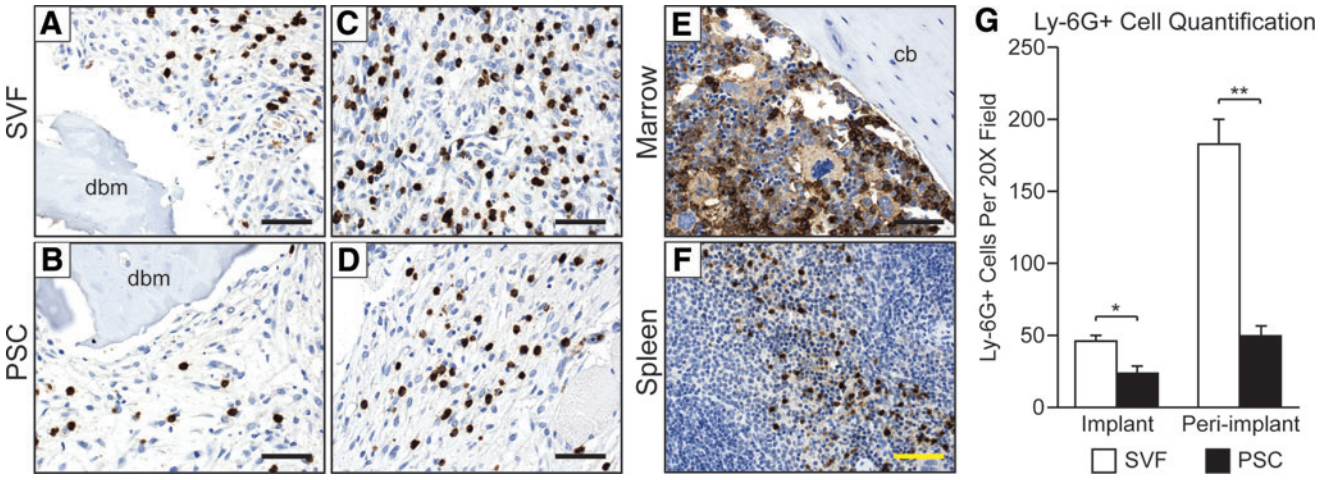

FIG. 3. Ly-6G immunohistochemistry within early time points of SVF or PSC intramuscular implantation. Ly-6G immunostaining (appearing *brown*) highlights peripheral granulocytes, as well as most myeloid cells within the bone marrow. Nuclear counterstain appears *blue*. **(A, B)** High-magnification images of Ly-6G immunostaining within the implant site, 1 week postoperatively. 40× images. Scale bar (*black*) = 25 μM. **(C, D)** High-magnification images of Ly-6G immunostaining within the immediate peri-implant area, 1 week postoperatively. 40× images. Scale bar (*black*) = 25 μM. **(E)** Ly-6G immunostaining within the mouse bone marrow, serving as an internal control and highlight the majority of myeloid cells. 40× images. Scale bar (*black*) = 25 μM. **(F)** Ly-6G immunostaining within the mouse spleen, serving as a further control tissue. 20× images. Scale bar (*yellow*) = 50 μM. **(G)** Quantification of Ly-6G$^+$ cell number, as assessed per random 20× field within the implant site and immediate peri-implant areas. $*p < 0.05$; $**p < 0.01$. $n = 4$ implants per cell treatment; $n = 10$ images analyzed per sample. Color images available online at www.liebertpub.com/tea

Immunomodulatory effects of PSC in an immunocompetent animal model

Next, and to verify the applicability of our findings, we sought to extend our observations to an immunocompetent animal model (Supplementary Fig. S1). Here, an absorbable collagen sponge implant was used, treated without cells (acellular, Supplementary Fig. S1A–D), with SVF (Supplementary Fig. S1E–H), or patient-identical PSC (Supplementary Fig. S1I–L). The acellular scaffold alone resulted in a mild postoperative inflammatory reaction. Minimal inflammatory cells were observed in the mid-substance of the

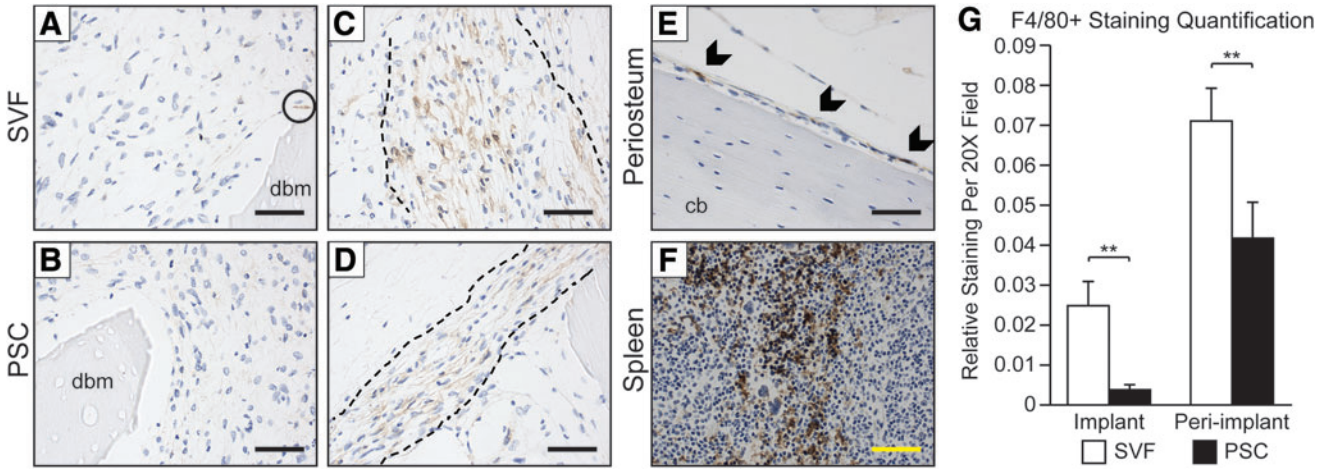

FIG. 4. F4/80 immunohistochemistry within early time points of SVF or PSC intramuscular implantation. F4/80 immunostaining (appearing *brown*) highlights macrophages. Nuclear counterstain appears *blue*. **(A, B)** High-magnification images of F4/80 immunostaining within the implant site, 1 week postoperatively. Rare to scattered individual cells stained, primarily next to dbm particles. 40× images. Scale bar (*black*) = 25 μM. *Circle* indicates area of positive staining for F4/80. **(C, D)** High-magnification images of F4/80 immunostaining within the immediate peri-implant area, 1 week postoperatively. A band-like area of F4/80 immunoreactivity was observed encircling the implant site (margins indicated by *dashed black lines*). 40× images. Scale bar (*black*) = 25 μM. **(E)** F4/80 immunostaining within the mouse periosteum, serving as an internal control and highlighting periosteal macrophages. Scale bar (*black*) = 25 μM. *Arrowheads* indicate areas of positive staining for F4/80. **(F)** F4/80 immunostaining within the mouse spleen, serving as a further control tissue. 20× images. Scale bar (*yellow*) = 50 μM. **(G)** Quantification of F4/80 relative intensity of staining, as assessed per random 20× field within the implant site and immediate peri-implant areas. $**p < 0.01$. $n = 4$ implants per cell treatment; $n = 10$ images analyzed per sample. Color images available online at www.liebertpub.com/tea

scaffold (s) (Supplementary Fig. S1A), mild mixed inflammation was observed as the scaffold edge (Supplementary Fig. S1B) along with edema in the immediately adjacent tissue planes (Supplementary Fig. S1C). Larger neural (n) and vascular (v) structures adjacent to the implant were largely free of inflammation (Supplementary Fig. S1D). Both cell implant types (SVF and PSC) showed increased inflammation in comparison to acellular control. However, an exaggerated inflammatory response to SVF-laden implants was again observed in comparison to PSC-laden implants. These differences were observable in the scaffold mid-substance (Supplementary Fig. S1E, I), scaffold edge (Supplementary Fig. S1F, G, J, K), as well as in surrounding neurovascular structures (Supplementary Fig. S1H, L). In summary, an exaggerated early inflammatory infiltrate was observed with SVF treatment across SCID and immunocompetent animal models of ectopic bone formation.

PSC express anti-inflammatory cytokines

To gain more insight into the specific inflammatory pathways modulated by human SVF and PSC after implantation, we examined in patient-identical SVF and PSC cell isolates an array of genes involved in the early inflammatory response using qRT-PCR. Genes analyzed included interleukins (*IL-1α, IL-1β, IL-4, IL-6, I-L8, IL-10, IL-12α, IL-12 β, IL-13,* and *IL-18),* tumor necrosis factor-alpha *(TNF- α),* and interferon gamma *(IFN-γ)* (Table 1). As expected, the expression of proinflammatory cytokines was highly upregulated in the SVF cell isolate as compared with purified PSC, including *IL-1α, IL-1β, IL-8, IL-18, TNF-α,* and *IFN-γ*. Among the most prominent proinflammatory genes expressed among SVF were *IL-1α, IL-1β, and IFN-γ,* expressed in the SVF at 386-, 843-, and 505-fold greater than in patient-identical PSC. These findings are likely attributable to the FACS-based removal of $CD45^+$ cells, which removes nearly all inflammatory cells among SVF. Conversely, several markers, which regulate or inhibit the inflammatory response, were upregulated among PSC. For example, the anti-inflammatory cytokine *IL-10*[34] and regulatory/pleiotropic cytokine *IL-6*[35] were more highly expressed in the PSC group. Thus, expression of inflammatory cytokines widely differs by method of cell preparation. The unpurified SVF contains a high level of proinflammatory cytokines, whereas purified preparations of PSC have higher levels of *IL-6* and *IL-10*.

Discussion

In summary, differences in the bone-forming potential of patient-matched SVF and PSC are inversely related to the innate inflammatory infiltrate within the early postoperative period. Specifically, we have shown that human PSC are superior to unsorted SVF in bone formation outcomes,[17] and that this is accompanied by a muted early infiltration of granulocytes and macrophages into the implant area.

Multiple differences between PSC and SVF implantation have been previously reported. Bone formation has been documented to be significantly greater within PSC-laden implants, documented by both radiographic imaging and microCT-based quantification, as well as histomorphometric analysis and detection of key bone-specific antigens such as osteocalcin.[17] Importantly, PSC appear to be the effector cell type for bone formation, confirmed by both human-specific antigen expression, as well as cell tracking studies with fluorescent labeling, although host osteoprogenitor cells also participate.[17] Differences in vascularization have also been noted among PSC-laden implants.[20] Here, semiquantitative histomorphometric analysis of intramuscular implants showed a significant increase in mean blood vessel numbers and blood vessel area, along with immunohistochemical evidence of increased vascular endothelial growth factor elaboration.[20] In aggregate, these studies found that adipose-derived PSC induce greater amounts of vascularized bone formation than their unpurified stromal counterpart, even when derived from the same patient sample. A link between the pro-osteogenic/provasculogenic effects of PSC and anti-inflammatory effects had not yet been established.

The relationship between inflammation and MSC-mediated bone formation is complex, and the literature is scattered with contradictory reports (see Deshpande *et al.*[36] for a review). When studied in isolation, inflammatory cytokines either inhibit or enhance MSC osteogenic differentiation in a dose- and context-dependent fashion.[36] However, it is becoming clearer that an unrestrained inflammatory response, especially when sustained, induces an inhibitory effect on osteoblastogenesis

Table 1. Relative Expression of Early Inflammatory Genes in Human Adipose Tissue Derived Stromal Vascular Fraction and Perivascular Stem/Stromal Cells

Gene	*SVF*	*PSC*	*Relative expression (SVF/PSC)*	*Benjamini–Hochberg* p-*value*	*Significance*
IL-1α	1.002	0.003	386.02	0.00016	**
IL-1β	1.005	0.001	843.11	0.00037	**
IL-4	1.370	0.141	9.74	0.10767	NS
IL-6	1.003	2.670	0.38	0.00536	**
IL-8	1.061	0.059	17.83	0.00147	**
IL-10	1.001	3.968	0.25	0.00070	**
IL-12α	1.045	1.146	0.91	0.40810	NS
IL-12β	1.315	0.271	4.84	0.22649	NS
IL-13	1.509	0.353	4.28	0.01566	*
IL-18	1.005	0.054	18.62	0.00048	**
TNF-α	1.002	0.020	49.30	0.00016	**
IFN-γ	1.003	0.002	505.72	0.00021	**

*$p < 0.05$; **$p < 0.01$.
NS, no significant; PSC, perivascular stem/stromal cells; SVF, stromal vascular fraction.

and bone formation.[37] Therefore, it is possible that human SVF implantation, which is ~1/3rd inflammatory cells, sets in motion an innate immune response that is detrimental to cell survival and/or osteogenic differentiation within the implantation site. In the current study, an exaggerated early inflammatory reaction in the SVF group may be largely attributed to the high expression of proinflammatory cytokines, such as *IL-1β*, *TNF-α*, and *IFN-γ*. Interestingly, high concentrations of all these factors have been previously shown to have inhibitory effects on MSC osteogenic differentiation.[38–40] Although only speculation, specific Ly-6G neutralizing antibodies have been used with success,[41] and could be used to complement SVF implantation in an attempt to mute a detrimental inflammatory response.

PSC implantation has been examined in both ectopic models of bone formation, such as the intramuscular model studied here[17] as well as bone defect/repair models.[15,16] Intramuscular models of bone formation pose several advantages for experimentation, including ease of surgical instrumentation, wide use, capacity for larger volume implants, and experimental reproducibility (reviewed in Scott *et al.*[42]). The present study found that PSC induced a marked reduction in innate inflammatory cell infiltrates when implanted in a muscle pouch. These immunomodulatory effects of PSC may be partially attributed to the increased expression of the anti-inflammatory cytokine, *IL-10*, which selectively inhibits macrophage and natural killer (NK) cell production of proinflammatory cytokines.[43] Future studies will examine if PSC inhibit the early immune response in the same manner when implanted in a bone defect environment.

Importantly, several limitations to the above study exist. First and foremost, the majority of studies were performed in SCID mice so as to all xenografting of human cells. Recognizing the altered immune environment in SCID mice, we focused solely on analysis of members of the innate immune system, including granulocytes and macrophages. Despite the lack of B and T lymphocytes, SCID mice have normal development and normal number of phagocytic cells, including macrophages and neutrophils.[44] In this regard, the genetic mutation in SCID mice has no direct effects on innate immunity. However, some studies suggest indirect effects on phagocytic function. For example, reduced T lymphocyte-derived cytokine production may result in impaired opsonization and phagocytic efficiency.[45] Of course, there are T cell independent mechanisms of macrophage activation, such as through NK cells.[46] NK cells are in fact present in higher numbers in SCID mice, and NK cell-mediated macrophage activation may compensate for T cell deficiency.[46,47] Additional studies were performed in a corollary immunocompetent model, largely replicating our prior findings. However, these studies likewise have some inherent limitations as they represent a xenograft model in an immunocompetent animal. Future in-depth exploration of this difference in early postoperative inflammation would require a validated murine PSC cell population.

Another limitation results from the heterogeneity of PSC, although PSC are relatively homogenous in comparison to an unsorted stromal cell population, some degree of heterogeneity of course exists even within this FACS-derived population. First, from a definitional standpoint, PSC represents a bipartite population of two related populations: pericytes and adventitial cells. Current theories suggest that adventitial cells are a more undifferentiated cell type,[48] and that under appropriate conditions adventitial cells can adopt a pericyte-like phenotype.[19] As well, other investigators have clearly shown that the pericyte population is able to be further segregated *in vivo* based on a several markers, including smooth muscle actin,[19] NG2,[49–52] and nestin.[49–52] Moreover, Sacchetti *et al.* recently reported that anatomic site of origin seems to partially dictate the lineage differentiation potential of $CD146^+$ pericytes.[53] In other examples of anatomic specification, we have shown that a subset of cardiac pericytes express cardiomyogenic potential,[54] pericytes from the infrapatellar fat pad exhibit much higher chondrogenic potential than their counterparts in other fat depots,[55] and that a subset of kidney pericytes are committed to renin secretion.[56] The extent to which one or more cell types within PSC have unique immunomodulatory attributes is as yet unknown.

In summary, human PSC are superior to unsorted SVF in bone formation outcomes, and this is accompanied by a muted early infiltration of granulocytes and macrophages into the implant area. Adipose-derived PSC are readily obtainable from human lipoaspirate without the need for culture, and may be used for future efforts in clinical bone translation.

Acknowledgments

The present work was supported by the NIH/NIAMS (grants R01 AR061399, R01 AR066782, K08 AR068316), the Musculoskeletal Transplant Foundation, the Maryland Stem Cell Research Fund, and Orthopedic Research and Education Foundation with funding provided by the Musculoskeletal Transplant Foundation. The authors thank P. Giacomelli for her excellent technical assistance.

Authors Contributions

C.A.M.: collection and/or assembly of data, article writing; J.X.: collection and/or assembly of data; L.Z.: collection and/or assembly of data; G.A.: collection and/or assembly of data; C.D.: collection and/or assembly of data; N.Y.: collection and/or assembly of data; K.B.: provision of study material; J.S.: provision of study material; R.G.: collection and/or assembly of data; X.Z.: collection and/or assembly of data; K.T.: provision of study material, financial support; C.S.: provision of study material, financial support; B.P.: provision of study material; A.W.J.: provision of study material, financial support, and final approval of the article.

Disclosure Statement

K.T., B.P., and C.S. are inventors of perivascular stromal cell-related patents filed from UCLA. K.T. and C.S. are founders of Scarless Laboratories, Inc. which sublicenses perivascular stromal cell-related patents from the UC Regents, and who also hold equity in the company. C.S. is also an officer of Scarless Laboratories, Inc. The other authors have no competing financial interests.

References

1. Allt, G., and Lawrenson, J.G. Pericytes: cell biology and pathology. Cells Tissues Organs **169,** 1, 2001.
2. Collett, G.D., and Canfield, A.E. Angiogenesis and pericytes in the initiation of ectopic calcification. Circ Res **96,** 930, 2005.

3. Doherty, M.J., and Canfield, A.E. Gene expression during vascular pericyte differentiation. Crit Rev Eukaryot Gene Expr **9,** 1, 1999.
4. Farrington-Rock, C., Crofts, N.J., Doherty, M.J., Ashton, B.A., Griffin-Jones, C., and Canfield, A.E. Chondrogenic and adipogenic potential of microvascular pericytes. Circulation **110,** 2226, 2004.
5. Covas, D.T., Piccinato, C.E., Orellana, M.D., Siufi, J.L., Silva, W.A., Jr., Proto-Siqueira, R., Rizzatti, E.G., Neder, L., Silva, A.R., Rocha, V., and Zago, M.A. Mesenchymal stem cells can be obtained from the human saphena vein. Exp Cell Res **309,** 340, 2005.
6. Crisan, M., Yap, S., Casteilla, L., Chen, C.W., Corselli, M., Park, T.S., Andriolo, G., Sun, B., Zheng, B., Zhang, L., Norotte, C., Teng, P.N., Traas, J., Schugar, R., Deasy, B.M., Badylak, S., Buhring, H.J., Giacobino, J.P., Lazzari, L., Huard, J., and Peault, B. A perivascular origin for mesenchymal stem cells in multiple human organs. Cell Stem Cell **3,** 301, 2008.
7. Murray, I.R., West, C.C., Hardy, W.R., James, A.W., Park, T.S., Nguyen, A., Tawonsawatruk, T., Lazzari, L., Soo, C., and Peault, B. Natural history of mesenchymal stem cells, from vessel walls to culture vessels. Cell Mol Life Sci **71,** 1353, 2014.
8. Tang, W., Zeve, D., Suh, J.M., Bosnakovski, D., Kyba, M., Hammer, R.E., Tallquist, M.D., and Graff, J.M. White fat progenitor cells reside in the adipose vasculature. Science **322,** 583, 2008.
9. Feng, J., Mantesso, A., De Bari, C., Nishiyama, A., and Sharpe, P.T. Dual origin of mesenchymal stem cells contributing to organ growth and repair. Proc Natl Acad Sci U S A **108,** 6503, 2011.
10. Dellavalle, A., Sampaolesi, M., Tonlorenzi, R., Tagliafico, E., Sacchetti, B., Perani, L., Innocenzi, A., Galvez, B.G., Messina, G., Morosetti, R., Li, S., Belicchi, M., Peretti, G., Chamberlain, J.S., Wright, W.E., Torrente, Y., Ferrari, S., Bianco, P., and Cossu, G. Pericytes of human skeletal muscle are myogenic precursors distinct from satellite cells. Nat Cell Biol **9,** 255, 2007.
11. Zuk, P.A., Zhu, M., Ashjian, P., De Ugarte, D.A., Huang, J.I., Mizuno, H., Alfonso, Z.C., Fraser, J.K., Benhaim, P., and Hedrick, M.H. Human adipose tissue is a source of multipotent stem cells. Mol Biol Cell **13,** 4279, 2002.
12. Zuk, P.A. The adipose-derived stem cell: looking back and looking ahead. Mol Biol Cell **21,** 1783, 2010.
13. Levi, B., Wan, D.C., Glotzbach, J.P., Hyun, J., Januszyk, M., Montoro, D., Sorkin, M., James, A.W., Nelson, E.R., Li, S., Quarto, N., Lee, M., Gurtner, G.C., and Longaker, M.T. CD105 protein depletion enhances human adipose-derived stromal cell osteogenesis through reduction of transforming growth factor beta1 (TGF-beta1) signaling. J Biol Chem **286,** 39497, 2011.
14. Jiang, T., Liu, W., Lv, X., Sun, H., Zhang, L., Liu, Y., Zhang, W.J., Cao, Y., and Zhou, G. Potent in vitro chondrogenesis of CD105 enriched human adipose-derived stem cells. Biomaterials **31,** 3564, 2010.
15. Chung, C.G., James, A.W., Asatrian, G., Chang, L., Nguyen, A., Le, K., Bayani, G., Lee, R., Stoker, D., Zhang, X., Ting, K., Péault, B., and Soo, C. Human perivascular stem cell-based bone graft substitute induces rat spinal fusion. Stem Cells Transl Med **3,** 1231, 2014.
16. James, A.W., Zara, J.N., Corselli, M., Askarinam, A., Zhou, A.M., Hourfar, A., Nguyen, A., Megerdichian, S., Asatrian, G., Pang, S., Stoker, D., Zhang, X., Wu, B., Ting, K., Péault, B., and Soo, C. An abundant perivascular source of stem cells for bone tissue engineering. Stem Cells Transl Med **1,** 673, 2012.
17. James, A.W., Zara, J.N., Zhang, X., Askarinam, A., Goyal, R., Chiang, M., Yuan, W., Chang, L., Corselli, M., Shen, J., Pang, S., Stoker, D., Wu, B., Ting, K., Péault, B., and Soo, C. Perivascular stem cells: a prospectively purified mesenchymal stem cell population for bone tissue engineering. Stem Cells Transl Med **1,** 510, 2012.
18. West, C.C., Hardy, W.R., Murray, I.R., James, A.W., Corselli, M., Pang, S., Black, C., Lobo, S.E., Sukhija, K., Liang, P., Lagishetty, V., Hay, D.C., March, K.L., Ting, K., Soo, C., and Péault, B. Prospective purification of perivascular presumptive mesenchymal stem cells from human adipose tissue: process optimization and cell population metrics across a large cohort of diverse demographics. Stem Cell Res Ther **7,** 47, 2016.
19. Corselli, M., Chen, C.W., Sun, B., Yap, S., Rubin, J.P., and Péault, B. The tunica adventitia of human arteries and veins as a source of mesenchymal stem cells. Stem Cells Dev **21,** 1299, 2012.
20. Askarinam, A., James, A.W., Zara, J.N., Goyal, R., Corselli, M., Pan, A., Liang, P., Chang, L., Rackohn, T., Stoker, D., Zhang, X., Ting, K., Péault, B., and Soo, C. Human perivascular stem cells show enhanced osteogenesis and vasculogenesis with Nel-like molecule I protein. Tissue Eng Part A **19,** 1386, 2013.
21. James, A.W., Zara, J.N., Corselli, M., Chiang, M., Yuan, W., Nguyen, V., Askarinam, A., Goyal, R., Siu, R.K., Scott, V., Lee, M., Ting, K., Péault, B., and Soo, C. Use of human perivascular stem cells for bone regeneration. J Vis Exp e2952, 2012.
22. Hurtado-Alvarado, G., Cabanas-Morales, A.M., and Gomez-Gonzalez, B. Pericytes: brain-immune interface modulators. Front Integr Neurosci **7,** 80, 2014.
23. Pieper, C., Marek, J.J., Unterberg, M., Schwerdtle, T., and Galla, H.J. Brain capillary pericytes contribute to the immune defense in response to cytokines or LPS in vitro. Brain Res **1550,** 1, 2014.
24. Ochs, K., Sahm, F., Opitz, C.A., Lanz, T.V., Oezen, I., Couraud, P.O., von Deimling, A., Wick, W., and Platten, M. Immature mesenchymal stem cell-like pericytes as mediators of immunosuppression in human malignant glioma. J Neuroimmunol **265,** 106, 2013.
25. Frangogiannis, N.G. Regulation of the inflammatory response in cardiac repair. Circ Res **110,** 159, 2012.
26. Maier, C.L., and Pober, J.S. Human placental pericytes poorly stimulate and actively regulate allogeneic CD4 T cell responses. Arterioscler Thromb Vasc Biol **31,** 183, 2011.
27. Bose, A., Barik, S., Banerjee, S., Ghosh, T., Mallick, A., Bhattacharyya Majumdar, S., Goswami, K.K., Bhuniya, A., Banerjee, S., Baral, R., Storkus, W.J., Dasgupta, P.S., and Majumdar, S. Tumor-derived vascular pericytes anergize Th cells. J Immunol **191,** 971, 2013.
28. Ma, H.L., Blanchet, T.J., Peluso, D., Hopkins, B., Morris, E.A., and Glasson, S.S. Osteoarthritis severity is sex dependent in a surgical mouse model. Osteoarthritis Cartilage **15,** 695, 2007.
29. Bobryshev, Y.V., Moisenovich, M.M., Pustovalova, O.L., Agapov, I.I., and Orekhov, A.N. Widespread distribution of HLA-DR-expressing cells in macroscopically undiseased intima of the human aorta: a possible role in surveillance and maintenance of vascular homeostasis. Immunobiology **217,** 558, 2012.
30. Murray, A.G., Libby, P., and Pober, J.S. Human vascular smooth muscle cells poorly co-stimulate and actively inhibit allogeneic CD4+ T cell proliferation in vitro. J Immunol **154,** 151, 1995.
31. Chen, C.W., Okada, M., Proto, J.D., Gao, X., Sekiya, N., Beckman, S.A., Corselli, M., Crisan, M., Saparov, A.,

Tobita, K., Péault, B., and Huard, J. Human pericytes for ischemic heart repair. Stem Cells **31,** 305, 2013.
32. Bender, S.A., Rogalski, J.B., Mills, M.P., Arnold, R.M., Cochran, D.L., and Mellonig, J.T. Evaluation of demineralized bone matrix paste and putty in periodontal intraosseous defects. J Periodontol **76,** 768, 2005.
33. Han, B., Tang, B., and Nimni, M.E. Quantitative and sensitive in vitro assay for osteoinductive activity of demineralized bone matrix. J Orthop Res **21,** 648, 2003.
34. Murray, P.J. The primary mechanism of the IL-10-regulated antiinflammatory response is to selectively inhibit transcription. Proc Natl Acad Sci U S A **102,** 8686, 2005.
35. Hunter, C.A., and Jones, S.A. IL-6 as a keystone cytokine in health and disease. Nat Immunol **16,** 448, 2015.
36. Deshpande, S., James, A.W., Blough, J., Donneys, A., Wang, S.C., Cederna, P.S., Buchman, S.R., and Levi, B. Reconciling the effects of inflammatory cytokines on mesenchymal cell osteogenic differentiation. J Surg Res **185,** 278, 2013.
37. Xu, J., Wang, Y., Li, J., Zhang, X., Geng, Y., Huang, Y., and Dai, K. IL-12p40 impairs mesenchymal stem cell-mediated bone regeneration via CD4(+) T cells. Cell Death Differ **23,** 1941, 2016.
38. Huang, H., Zhao, N., Xu, X., Xu, Y., Li, S., Zhang, J., and Yang, P. Dose-specific effects of tumor necrosis factor alpha on osteogenic differentiation of mesenchymal stem cells. Cell Prolif **44,** 420, 2011.
39. Dighe, A.S., Yang, S., Madhu, V., Balian, G., and Cui, Q. Interferon gamma and T cells inhibit osteogenesis induced by allogeneic mesenchymal stromal cells. J Orthop Res **31,** 227, 2013.
40. Mao, C.Y., Wang, Y.G., Zhang, X., Zheng, X.Y., Tang, T.T., and Lu, E.Y. Double-edged-sword effect of IL-1beta on the osteogenesis of periodontal ligament stem cells via crosstalk between the NF-kappaB, MAPK and BMP/Smad signaling pathways. Cell Death Dis **7,** e2296, 2016.
41. Daley, J.M., Thomay, A.A., Connolly, M.D., Reichner, J.S., and Albina, J.E. Use of Ly6G-specific monoclonal antibody to deplete neutrophils in mice. J Leukoc Biol **83,** 64, 2008.
42. Scott, M.A., Levi, B., Askarinam, A., Nguyen, A., Rackohn, T., Ting, K., Soo, C., and James, A.W. Brief review of models of ectopic bone formation. Stem Cells Dev **21,** 655, 2012.
43. Couper, K.N., Blount, D.G., and Riley, E.M. IL-10: the master regulator of immunity to infection. J Immunol **180,** 5771, 2008.
44. Bancroft, G.J., and Kelly, J.P. Macrophage activation and innate resistance to infection in SCID mice. Immunobiology **191,** 424, 1994.
45. Arango Duque, G., and Descoteaux, A. Macrophage cytokines: involvement in immunity and infectious diseases. Front Immunol **5,** 491, 2014.
46. Bancroft, G.J., Schreiber, R.D., and Unanue, E.R. T cell-independent macrophage activation in scid mice. Curr Top Microbiol Immunol **152,** 235, 1989.
47. Hu, X., Liu, G., Hou, Y., Shi, J., Zhu, L., Jin, D., Peng, J., and Zhao, Y. Induction of M2-like macrophages in recipient NOD-scid mice by allogeneic donor CD4(+)CD25(+) regulatory T cells. Cell Mol Immunol **9,** 464, 2012.
48. Hardy, W.R., Moldovan, N.I., Moldovan, L., Livak, K.J., Datta, K., Goswami, C., Corselli, M., Traktuev, D.O., Murray, I.R., Peault, B., and March, K. Transcriptional networks in single perivascular cells sorted from human adipose tissue reveal a hierarchy of mesenchymal stem cells. Stem Cells **35,** 1273, 2017.
49. Birbrair, A., Zhang, T., Files, D.C., Mannava, S., Smith, T., Wang, Z.M., Messi, M.L., Mintz, A., and Delbono, O. Type-1 pericytes accumulate after tissue injury and produce collagen in an organ-dependent manner. Stem Cell Res Ther **5,** 122, 2014.
50. Birbrair, A., Zhang, T., Wang, Z.M., Messi, M.L., Enikolopov, G.N., Mintz, A., and Delbono, O. Skeletal muscle pericyte subtypes differ in their differentiation potential. Stem Cell Res **10,** 67, 2013.
51. Birbrair, A., Zhang, T., Wang, Z.M., Messi, M.L., Olson, J.D., Mintz, A., and Delbono, O. Type-2 pericytes participate in normal and tumoral angiogenesis. Am J Physiol Cell Physiol **307,** C25, 2014.
52. Birbrair, A., Zhang, T., Wang, Z.M., Messi, M.L., Enikolopov, G.N., Mintz, A., and Delbono, O. Role of pericytes in skeletal muscle regeneration and fat accumulation. Stem Cells Dev **22,** 2298, 2013.
53. Sacchetti, B., Funari, A., Remoli, C., Giannicola, G., Kogler, G., Liedtke, S., Cossu, G., Serafini, M., Sampaolesi, M., Tagliafico, E., Tenedini, E., Saggio, I., Robey, P.G., Riminucci, M., and Bianco, P. No identical ''mesenchymal stem cells'' at different times and sites: human committed progenitors of distinct origin and differentiation potential are incorporated as adventitial cells in microvessels. Stem Cell Reports **6,** 897, 2016.
54. Chen, W.C., Baily, J.E., Corselli, M., Diaz, M.E., Sun, B., Xiang, G., Gray, G.A., Huard, J., and Peault, B. Human myocardial pericytes: multipotent mesodermal precursors exhibiting cardiac specificity. Stem Cells **33,** 557, 2015.
55. Hindle, P., Khan, N., Biant, L., and Peault, B. The infrapatellar fat pad as a source of perivascular stem cells with increased chondrogenic potential for regenerative medicine. Stem Cells Transl Med **6,** 77, 2017.
56. Stefanska, A., Kenyon, C., Christian, H.C., Buckley, C., Shaw, I., Mullins, J.J., and Péault, B. Human kidney pericytes produce renin. Kidney Int **90,** 1251, 2016.

Address correspondence to:
Aaron W. James, MD, PhD
Department of Pathology
Johns Hopkins University
Ross Research Building
Room 524A, 720 Rutland Avenue
Baltimore, MD 21205

E-mail: awjames@jhmi.edu

Chia Soo, MD, FACS
Division of Plastic and Reconstructive Surgery
Departments of Surgery and Orthopaedic Surgery
David Geffen School of Medicine
University of California, Los Angeles
675 Charles E. Young Dr. South
MacDonald, Research Laboratory Room 2641A
Los Angeles, CA 90095

E-mail: bsoo@ucla.edu

Received: January 11, 2017
Accepted: June 6, 2017
Online Publication Date: August 15, 2017